Journal of
www. biophotonics-journal.org
BIOPHOTONICS

WILEY-VCH

J. Biophotonics **4**, No. 7–8, 565–576 (2011) / **DOI** 10.1002/jbio.201000117

Journal of BIOPHOTONICS

FULL ARTICLE

Monitoring temporal development and healing of diabetic foot ulceration using hyperspectral imaging

Dmitry Yudovsky[1], *Aksone Nouvong*[2], *Kevin Schomacker*[3], *and Laurent Pilon*[*,1]

[1] University of California, Los Angeles, Henri Samueli School of Engineering and Applied Science, Biomedical Inter-Department Program, Los Angeles, CA 90095-1597, USA
[2] Department of Surgery 2B156 UCLA/Olive View Medical Center Sylmar, CA 91342-1495, USA also at Western University of Health Sciences
[3] HyperMed Inc., Burlington, MA 01803, USA

Received 13 December 2010, revised 25 January 2011, accepted 3 March 2011
Published online 1 April 2011

Key words: hyperspectral imaging, diabetic foot ulcer, tissue oximetry, medical screening technology, wound care, spectroscopy.

This study combines non-invasive hyperspectral imaging with an experimentally validated skin optical model and inverse algorithm to monitor diabetic feet of two representative patients. It aims to observe temporal changes in local epidermal thickness and oxyhemoglobin concentration and to gain insight into the progression of foot ulcer formation and healing. Foot ulceration is a debilitating comorbidity of diabetes that may result in loss of mobility and amputation. Inflammation and necrosis preempt ulceration and can result in changes in the skin prior to ulceration and during ulcer healing that affect oxygen delivery and consumption. Previous studies estimated oxyhemoglobin and deoxyhemoglobin concentrations around pre-ulcerative and ulcer sites on the diabetic foot using commercially available hyperspectral imaging systems. These measurements were successfully used to detect tissue at risk of ulceration and predict the healing potential of ulcers. The present study shows epidermal thickening and decrease in oxyhemoglobin concentration can also be detected prior to ulceration at pre-ulcerative sites. The algorithm was also able to observe reduction in the epidermal thickness combined with an increase in oxyhemoglobin concentration around the ulcer as it healed and closed. This methodology can be used for early prediction of diabetic foot ulceration in a clinical setting.

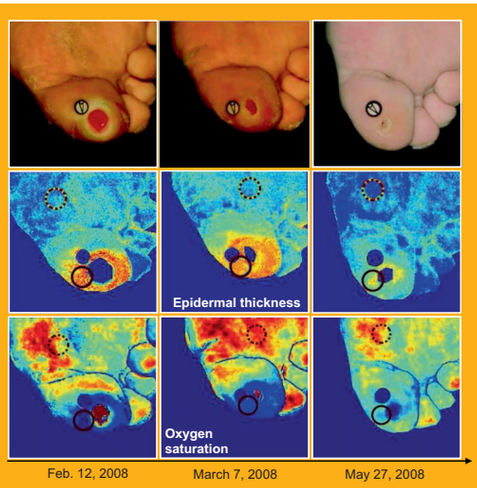

Healing process of a diabetic foot ulcer

1. Introduction

Diabetes mellitus affected 194 million people worldwide in 2004 [1] and is expected to increase in prevalence to 439 million by the year 2030 [2]. Foot ulceration is a major complication of diabetes mellitus and occurs in as many as 15–25% of patients with type 1 and 2 diabetes mellitus over their lifetime [3,

* Corresponding author: e-mail: pilon@seas.ucla.edu, Phone: +1 (310)-206-5598, Fax: +1 (310)-206-4830

Journal of
BIOPHOTONICS

4]. The cost of foot disorder diagnosis and management is estimated to be over 6 billion dollars annually in the United States [5, 6]. If left untreated, foot ulcers may become infected and develop deep tissue necrosis which may require amputation [7]. In fact, a foot ulcer precedes approximately 85% of all lower extremity amputations in patients with diabetes mellitus [7] and more than 88,000 lower limb amputations are performed annually on diabetic patients in the United States [8]. Hyperspectral imaging of the diabetic foot has been demonstrated to monitor vascular changes associated with diabetic neuropathy [9], ulcer healing [10], and ulcer formation [11]. This study explores the use of hyperspectral imaging and associated algorithms to monitor the temporal evolution of foot ulceration sites and to gain insight into the progression of foot ulcer formation and healing. Two patients for whom hyperspectral images were collected before, during and after foot ulceration are studied in details with particular attention paid to changes in epidermal thickness.

2. Background

Prolonged and poorly controlled diabetes irreparably damages bodily tissues. Nerve damage in the lower limbs results in diabetic neuropathy, whereby the patient's somatosensory and autonomic functions are diminished or completely lost [12, 13]. The subsequent loss of protective sensation, poor gait control, bone deformities, callus formation and inhibited sweat response result in excessive shear and pressure that damages the diabetic foot [14, 15]. Furthermore, 10 to 40% of diabetic patients are afflicted with peripheral vascular disease [16]. Typically, the vessels that carry blood to the legs, arms, stomach or kidneys narrow due to inflammation or tissue damage resulting in impaired blood flow to those regions [16]. Thus, repeated damage to the foot in conjunction with inhibited protective or healing response due to denervation or poor vascularization cause ulceration [13, 14, 16].

Recently, hyperspectral imaging in the visible and near-infrared parts of the spectrum has been used to determine the spatial distribution of oxygen saturation in human skin [17–19] and to detect the circulatory changes in the diabetic foot [10, 20, 21]. For example, Greenman et al. [9] used hyperspectral imaging to generate oxygen saturation and total hemoglobin concentration maps of the forearms and feet of type 1 and 2 diabetic subjects with and without diabetic neuropathy and of non-diabetic subjects without neurological disorders. The authors showed that the resting oxygen saturation averaged over the limb was lower among diabetic subjects with neuropathy than among both diabetic subjects without neuropathy and non-diabetic subjects. This suggests that diabetic neuropathy, which is a major contributor to ulceration [14, 15], could be detected by hyperspectral tissue oximetry.

In a different study, Khaodhiar et al. [20] measured *in vivo* oxyhemoglobin and deoxyhemoglobin concentrations using hyperspectral imaging near ulcer sites on the feet of type 1 diabetic patients. Hyperspectral imaging of the feet between 500 and 650 nm was performed at each visit for up to 4 times over a six month period. Then, the authors developed an ulcer healing prediction index based on the oxyhemoglobin and deoxyhemoglobin concentrations near the ulcer site which could distinguish ulcers that would heal from non-healing ulcers with a sensitivity and specificity of 93 and 86%, respectively.

Nouvong et al. [10] evaluated hyperspectral imaging as a tool for predicting the healing potential of diabetic foot ulcers on the feet of type 1 and 2 diabetic patients. Hyperspectral tissue oximetry measurements from feet of 66 diabetic patients were performed every two weeks for up to 18 months or until the ulcer healed. By measuring elevation and reduction in the average oxyhemoglobin concentration immediately around the ulcer area compared with adjacent tissue, the authors were able to predict the healing outcome of the formed ulcer with a sensitivity and specificity of 80 and 74%, respectively [10].

Yudovsky et al. [11] developed a predictive algorithm to automatically detect sites on the diabetic foot at risk of developing ulcers before visible signs of ulceration could be detected with the naked eye. This was achieved by retrospectively analyzing hyperspectral data collected by Nouvong et al. [10] 58 days, in average, before patients developed foot ulcers. An image processing algorithm based on this analysis was developed to automatically detect tissue that would ulcerate from tissue oximetry information. This algorithm was able to detect at-risk tissue with a sensitivity and specificity of 95 and 80%, respectively.

The studies previously described were limited to analysis of changes in oxyhemoglobin and deoxyhemoglobin concentrations and thus change in the circulatory function. Recently, Yudovsky and Pilon [22–24] developed a forward [22] and inverse method [23] to simultaneously determine, from diffuse reflectance spectra, (i) the melanin concentration and (ii) thickness of the epidermis, (iii) the volume fraction and oxygen saturation of blood in the dermis, and (iv) the scattering coefficient of skin [23, 24]. Their algorithm was validated on *in vivo* reflectance measurements from white and black subjects [24]. In the present study, changes in epidermal thickness on the diabetic foot were explored. Epidermal thickness can be measured reliably with punch biopsy whereby a sample of the skin is removed and analyzed *ex*

vivo [25, 26]. However, this invasive and destructive technique requires local anesthetic and should not be performed on diabetic feet to avoid the risk of causing an ulcer. Alternatively, non-invasive measurements of epidermal thickness can be made with techniques such as optical coherent tomography or ultrasound [27, 28]. However, these techniques are primarily sensitive to the tissue's scattering coefficient therefore simultaneous determination of chromophore concentrations is difficult if not impossible [29, 30]. Additionally, they do not provide a large enough field of view of the foot.

Finally, unlike previous studies which considered hyperspectral data collected during a single visit, this study investigates the sequences of hyperspectral images gathered before ulcer formation and during ulcer healing. In addition, hyperspectral data were analyzed with the method developed by Yudovsky and Pilon [23] to detect hyperkeratosis that preempt ulceration and monitor the evolution of the callus as the ulcer heals. Indeed, change in epidermal thickness at sites forming ulcers is of particular interest because (i) ulcer formation is frequently preceded by callus formation (epidermal thickening) and (ii) formed ulcers typically exhibit a thick callus ring spanning the permitter of the ulcer [14, 15].

3. Material and methods

3.1 Experimental data

Medical hyperspectral imaging consists of recording a series of images representing diffuse reflectance of biological tissue at discrete wavelengths λ_k resulting in a set of images called a hypercube denoted by $H(x, y, \lambda_k)$. Here, x and y are the spatial coordinates and λ_k is the spectral dimension. The hyperspectral imager used in this study is schematically depicted in Figure 1 and was described in detail in Ref. [11]. Two hypercubes were collected at each measurement site corresponding to either background or LED illuminated conditions denoted by $B_{\text{tissue}}(x, y, \lambda_k)$ and $M_{\text{tissue}}(x, y, \lambda_k)$, respectively. The LEDs were switched off and on to produce both illumination conditions, respectively. The spectral separator of the imager used in this study [11] was tuned to 15 equally spaced wavelengths between 500 and 660 nm while the CCD measured the tissue diffuse reflectance. Image acquisition at each wavelength lasted for approximately 1 second. A fiducial target was placed near the center of the imager's field of view to correct for patient movement during the image acquisition.

Spectral variation in external illumination intensity and CCD sensitivity were corrected by calibrating the hyperspectral imager to a well characterized highly reflective diffuse reflectance standard. This was performed prior to imaging each patient. The same procedure as above was used to acquire hypercubes of the calibration standard under background and LED illumination denoted by $B_{\text{calib}}(x, y, \lambda_k)$ and $M_{\text{calib}}(x, y, \lambda_k)$, respectively. Then, the diffuse reflectance measured at location (x, y) and wavelength λ_k was defined as

$$R_m(x, y, \lambda_k) = \frac{M_{\text{tissue}}(x, y, \lambda_k) - B_{\text{tissue}}(x, y, \lambda_k)}{M_{\text{calib}}(x, y, \lambda_k) - B_{\text{calib}}(x, y, \lambda_k)} \quad (1)$$

Note that hypercubes $B_{\text{tissue}}(x, y, \lambda_k)$ and $B_{\text{calib}}(x, y, \lambda_k)$ represent the reflectance of skin and the calibration standard, respectively, during background illumination only while the hypercubes $M_{\text{tissue}}(x, y, \lambda_k)$ and $M_{\text{calib}}(x, y, \lambda_k)$ represent the reflectance of skin and the calibration standard, respectively, illuminated by normally incident and collimated light and background illumination simultaneously.

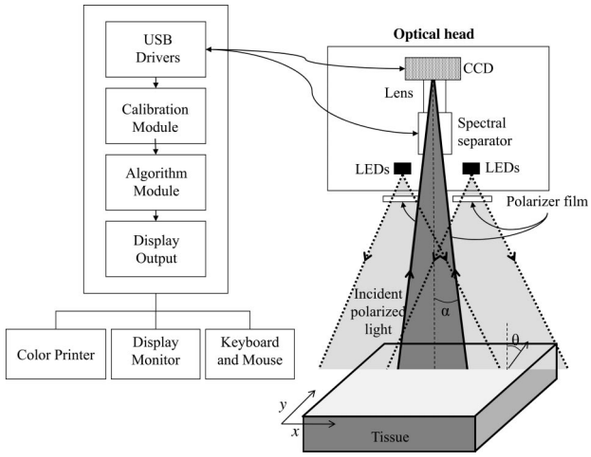

Figure 1 Schematic of the different components of the hyperspectral imager. The device acceptance angle α and exit angle θ are shown for reference.

3.2 Description of data set

Hyperspectral images were gathered from 66 subjects at the Olive View Medical Center (Olive View-UCLA IRB #05H-609300) as reported in detail in Ref. [10]. Each subject was (i) diagnosed with type 1 or 2 diabetes mellitus, (ii) afflicted with peripheral neuropathy [13, 14], and (iii) at risk of developing foot ulcers [4]. Twenty one subjects developed new ulcers during the course of the study [10]. Hyperspectral images of the feet of each subject were gathered over multiple visits. This study focuses on two representative subjects who exhibited foot ulceration

Journal of BIOPHOTONICS

on the planar aspect and toes of the foot. These representative subjects were chosen because more than two hyperspectral images were available for each ulceration phase, namely prior to and during ulceration as well as during ulcer healing.

3.3 Normal-hemispherical versus normal-normal reflectance

This section describes the relationship between the semi-empirical reflectance model for two-layer media developed by Yudovsky and Pilon [22], which predicts the normal-hemispherical reflectance denoted by $R_{n,h}(x,y,\lambda_k)$, and the diffuse reflectance $R_m(x,y,\lambda_k)$ measured by a finite aperture hyperspectral imager. The diffuse reflectance $R_m(x,y,\lambda_k)$ given by Eq. (1) can be expressed as [32],

$$R_m(x,y,\lambda_k) = \frac{2\pi\int_0^{\alpha} I_{\text{tissue}}(x,y,\lambda_k,\theta)\sin\theta\,\mathrm{d}\theta}{2\pi\int_0^{\alpha} I_{\text{calib}}(x,y,\lambda_k,\theta)\sin\theta\,\mathrm{d}\theta} \quad (2)$$

where $I_{\text{tissue}}(x,y,\lambda_k,\theta)$ and $I_{\text{calib}}(x,y,\lambda_k,\theta)$ are the intensities of light backscattered from skin and from the diffuse reflectance standard, respectively, into the solid angle $2\pi\,\mathrm{d}\theta$ around the polar angle θ and at coordinate (x,y) and wavelength λ_k. Furthermore, α is the acceptance angle of the hyperspectral imager's CCD as illustrated in Figure 1. As explained earlier, background illumination was removed in calculating $R_m(x,y,\lambda_k)$ by subtracting $B_{\text{tissue}}(x,y,\lambda_k)$ from $M_{\text{tissue}}(x,y,\lambda_k)$ and $B_{\text{calib}}(x,y,\lambda_k)$ from $M_{\text{calib}}(x,y,\lambda_k)$, respectively. Surface (or Fresnel) reflectance was removed by cross-polarizing the light emitted from the illumination LEDs relative to the liquid crystal spectral separator which is inherently polarized [11]. Thus, $I_{\text{tissue}}(x,y,\lambda_k,\theta)$ and $I_{\text{calib}}(x,y,\lambda_k,\theta)$ are the diffusely backscattered intensities under normal and collimated illumination.

The angular intensity of light backscattered from strongly scattering media such as skin exposed to normal and collimated irradiation has been shown to follow the Lambert's cosine law [33–35] given by [32],

$$I(x,y,\lambda_k,\theta) = \frac{R_{n,h}(x,y,\lambda_k)\cos\theta}{\pi} \quad (3)$$

where $R_{n,h}(x,y,\lambda_k)$ is the normal-hemispherical reflectance integrated over the outer hemisphere $(0 \le \theta \le \pi/2)$ and therefore, independent of θ. By substituting Eq. (3) into Eq. (2) for $I_{\text{tissue}}(x,y,\lambda_k,\theta)$ and $I_{\text{calib}}(x,y,\lambda_k,\theta)$ the diffuse reflectance $R_m(x,y,\lambda_k)$ can be expressed as

$$R_m(x,y,\lambda_k) = \frac{R_{n,h,\text{tissue}}(x,y,\lambda_k)}{R_{n,h,\text{calib}}(x,y,\lambda_k)} \quad (4)$$

where $R_{n,h,\text{tissue}}$ and $R_{n,h,\text{calib}}$ are the normal-hemispherical reflectance of skin and of the diffuse reflectance standard, respectively. Since the calibration standard is highly reflective for the wavelength range considered, $R_{n,h,\text{calib}}$ can be approximated to unity. Then, the measured reflectance $R_m(x,y,\lambda_k)$, given by Eq. (1), is equivalent to the normal-hemispherical reflectance $R_{n,h,\text{skin}}$, predicted by Yudovsky and Pilon [23], regardless of the acceptance angle α.

3.4 Tissue spectroscopy

Recently, Yudovsky and Pilon [24] developed an inverse method for determining the melanin concentration C_{mel}, blood volume fraction f_{blood}, oxygen saturation SO_2, epidermal thickness L_{epi}, and transport scattering coefficient $\mu_{s,tr}$ of human skin. The dependence of the transport scattering coefficient on wavelength was expressed as a power law: $\mu_{s,tr} = C(\lambda/\lambda_0)^b$ as implemented in Ref. [23]. The parameter C was assumed unknown while the parameters λ_0 and b were assumed to be 1 nm and 1.50, respectively. The biological characteristics of skin were assumed to be defined by a property vector $\vec{a}_e = (C_{\text{mel}}, L_{\text{epi}}, f_{\text{blood}}, \text{SO}_2, C)$. The goal of the inverse problem was to estimate the vector $\vec{a}_e$ at location (x,y) from the measured diffuse reflectance spectrum $R_m(x,y,\lambda_k)$. Tissue spectroscopy was achieved by finding an estimate vector $\vec{a}_e(x,y)$ that minimizes the sum of the squared residuals $r(x,y)$ expressed as [23],

$$r(x,y) = \sum_{k=1}^{K} [R_m(x,y,\lambda_k) - R_{n,h,\text{skin}}(x,y,\lambda_k,\vec{a}_e)]^2 \quad (5)$$

where $R_m(x,y,\lambda_k)$ was estimated experimentally using Eq. (1). The estimated normal-hemispherical reflectance of skin $R_{n,h,\text{skin}}(x,y,\lambda_k,\vec{a}_e)$ was evaluated using the semi-empirical model for two-layer media described in Ref. [22] [Eqs. (33) through (35)] as a function of $\vec{a}_e$. The residual $r(x,y)$ was minimized iteratively at each coordinate (x,y) using the constrained Levenberg-Marquardt algorithm [35]. Minimization was stopped once successive iterations of the algorithm no longer reduced $r(x,y)$ by more than 10^{-9} per iteration. This model has been validated against *in vivo* diffuse reflectance measurements of skin on the inner and outer forearm and forehead of subjects of white Caucasian and black African descent [24].

4. Results and discussion

4.1 Callus formation during ulceration

Figures 2 and 3 show visible images, oxygen saturation maps, epidermal thickness maps and oxyhemo-

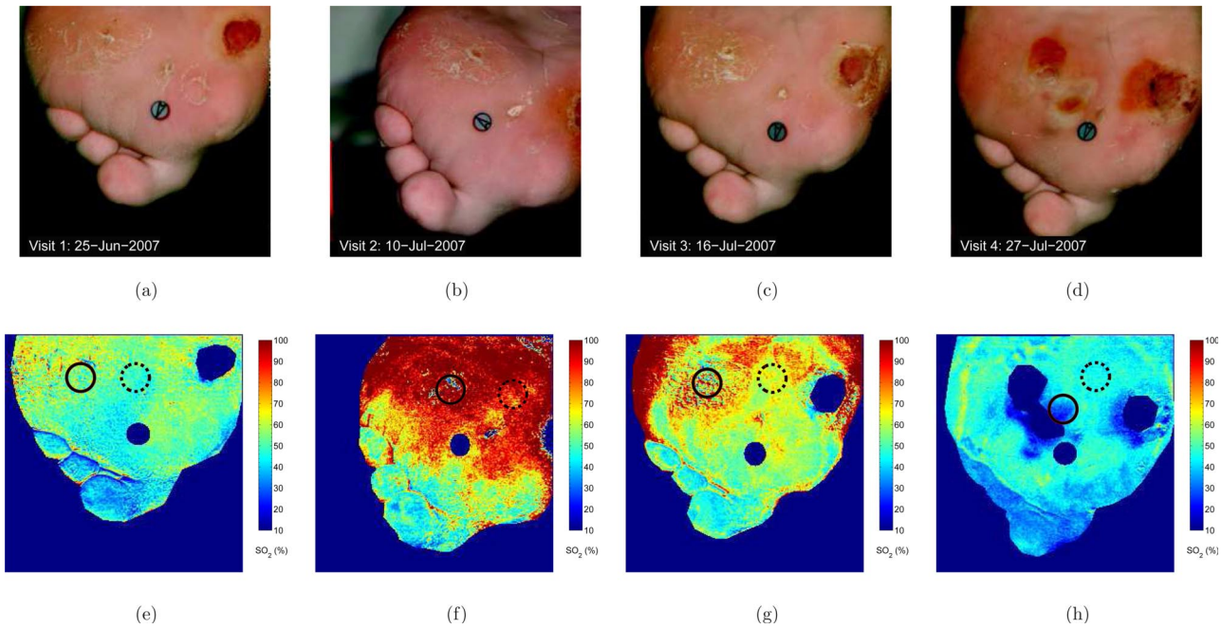

Figure 2 (online color at: www.biophotonics-journal.org) (**a**) to (**d**) Visible images and (**e**) to (**h**) oxygen saturation maps of the plantar surface of the right foot of a diabetic subject who developed a foot ulcer. Solid line circle indicates the ulceration site. Dashed line circle indicates the control site. Solid line circle indicates the ulceration site. Figures 2(a) through (d) represent the same time points as figures (e) through (h) during ulceration.

globin concentration maps of the plantar surface and toes of the right foot of a diabetic patient. The images were gathered over four visits during the course of one month. The patient exhibited an existing ulcer during the first visit over the first metatarsal head (Figure 2a) which persisted during the three following visits (Figures 2b through 2d). Furthermore, a new ulcer developed over the fourth metatarsal head between the third and fourth visit (Figure 2c).

Figures 2a through 2d show the visible image of the foot while Figures 2e through 2h show oxygen saturation maps estimated from the corresponding hyperspectral data. The estimated oxygen saturation SO_2 and epidermal thickness L_{epi} were averaged over an area 1 cm in diameter centered on the preulcer region over the fourth metatarsal head (solid line circle) and a control region over the second metatarsal head (dashed line circle) for each of the four visits. During visits 1, 2 and 3, the average SO_2 assessed over the ulcer was respectively, 80, 83, and 69% compared with 73, 95, and 72% for the control region. In a previous study [11] the range of oxygen saturation SO_2 at known preulcer sites was reported to be between 45 and 80%. This study [11] determined the oxygen saturation by comparing the apparent absorption of skin to reference apparent absorption spectra of fully saturated and desaturated blood and melanin solutions as described in Ref. [18]. The values of oxygen saturation determined in the present study were consistent with previous investigations even though different methods were used. The SO_2 value at the ulcer locations were found to be consistently lower compared to the control region during the visits leading up to ulceration. However, the absolute value of SO_2 varied significantly and without any apparent trend. For example, the average oxygen saturation assessed over the entire foot increased between visits 1 and 2 from 67 to 94%, but then decreased to 83% during visit 3. It was not expected that SO_2 values over the entire foot would be consistent from one visit to another as it fluctuates depending on the patient's activity. Therefore, we considered the relative difference in SO_2 between control and preulcer regions, measured during the same visit.

Figures 3a through 3d show the epidermal thickness maps of the plantar surface and toes of the right foot of a diabetic patient. They indicate that estimates of epidermal thickness varied between 70 and 170 μm. Note that L_{epi} was defined for an epidermis in which melanin was assumed to be homogeneously distributed throughout the entire layer [23]. In reality, melanin is concentrated close to the basement membrane and the majority of the epidermis is relatively transparent to visible light [36]. Assuming uniform melanin concentration may be acceptable for thin epidermis such as the forearm and forehead [24] but is less representative of epidermis on the foot. Indeed, histological studies of human skin from the sole of the foot have reported epidermal thick-

Journal of
BIOPHOTONICS

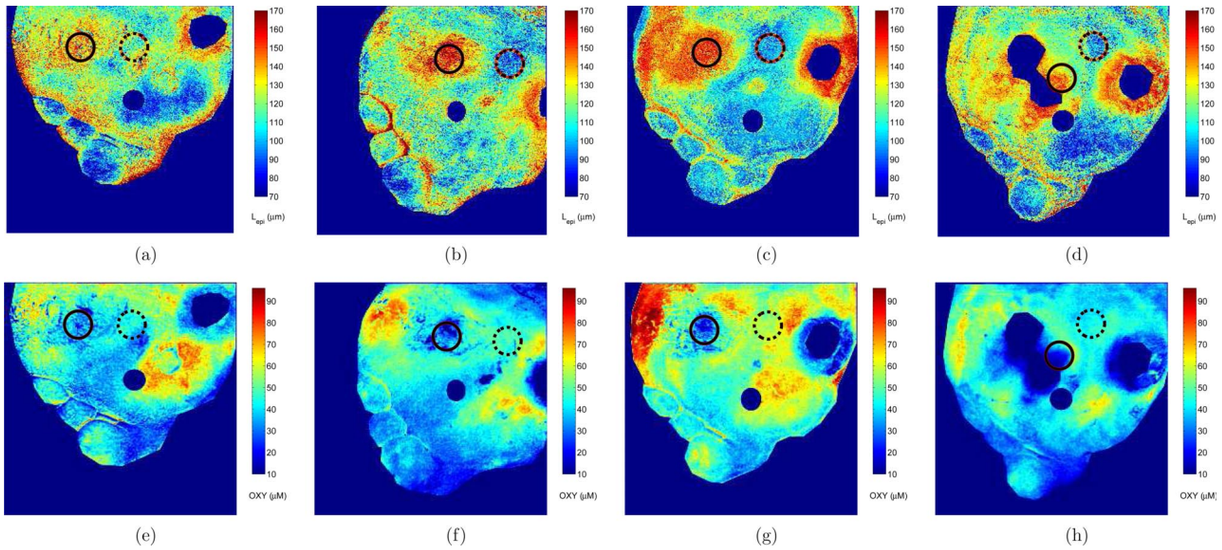

Figure 3 (online color at: www.biophotonics-journal.org) (**a**) to (**d**) Epidermal thickness and (**e**) to (**h**) oxyhemoglobin maps for the plantar surface of the same subject depicted in Figure 2. Solid line circle indicates the ulceration site. Dashed line circle indicates the control site. Figures 2(a) through (d) represent the same time points as figures (e) through (h) during ulceration.

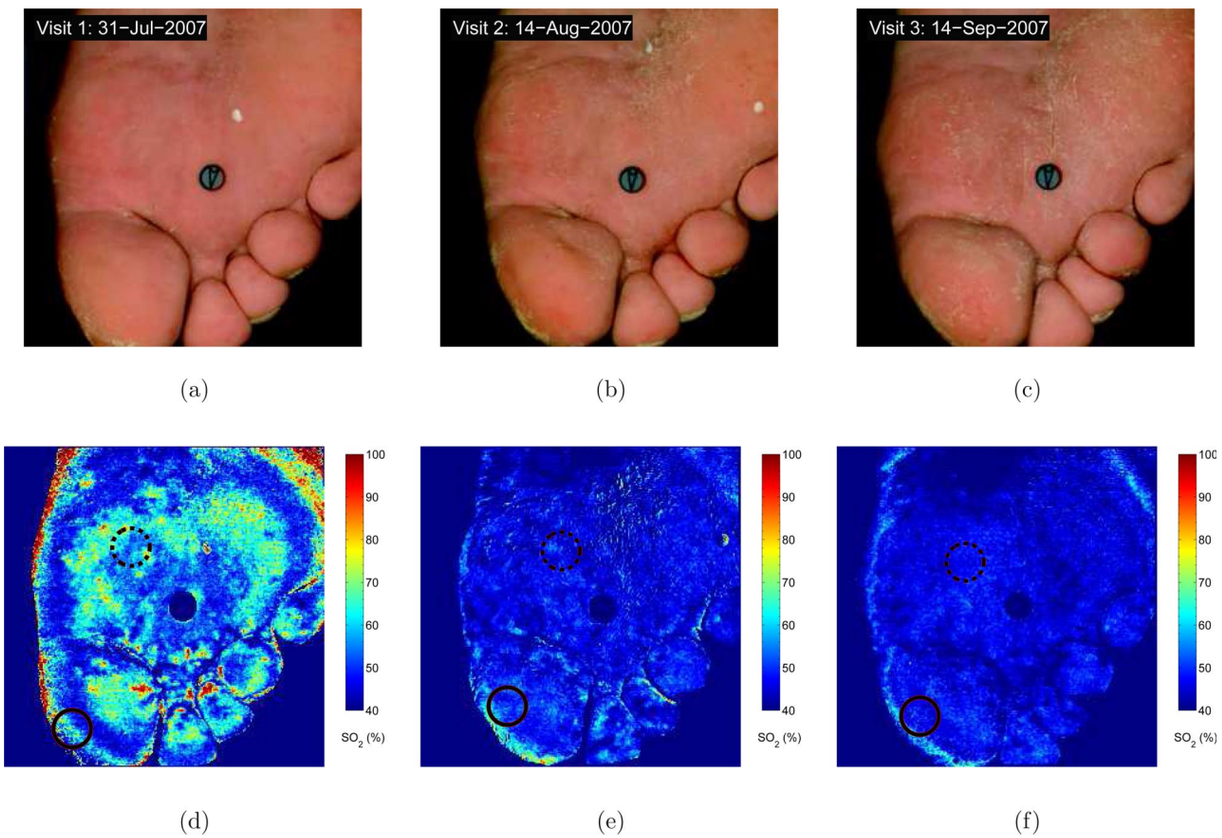

Figure 4 (online color at: www.biophotonics-journal.org) (**a**) to (**c**) Visible images and (**d**) to (**f**) oxygen saturation maps of the plantar surface of a diabetic subject during the development of a foot ulcer on the hallux of the left foot.

ness of up to 600 μm [38]. Thus, L_{epi} retrieved from diabetic feet was expected to be a relative estimate of the actual epidermal thickness on the plantar surface of the foot and not an exact value of the physical thickness. Nonetheless, Figures 2 and 3 show that the presence of callus around formed or forming ulcers (Figures 2a through 2d) consistently corresponds to an increase in the estimate of epidermal thickness L_{epi} (Figures 3a through 3d). Thus, L_{epi} retrieved is a relevant parameter that correlates with actual epidermal thickening. For each visit, the epidermis was consistently thicker in the preulcer region than in the unaffected control region and grew thicker over time. Quantitatively, the estimated average epidermal thickness in the preulcer region increased from 136, 157, to 159 μm during visits 1, 2, and 3, respectively, compared with 116, 93, and 98 μm at the unaffected control region during the same visits. The surface area of epidermal thickening where L_{epi} was greater than 140 μm increased from 3 cm^2 to 10 cm^2 between visits 2 and 3. Furthermore, the callus around the ulcer is visible during visit 4 as depicted in Figure 3d.

Figures 3e through 3h show the oxyhemoglobin concentration maps of the plantar surface and toes of the right foot of a diabetic patient. Interestingly, as the callus size and thickness increased between visits 1 and 3 (Figures 3a through 3c) the oxyhemoglobin concentration decreased (Figures 3e through 3g). In fact, the difference in average oxyhemoglobin concentration between the test and control sites was 8.01, −38.2, −36.4 and −108.3 μM during visits 1, 2, 3, and 4, respectively. This indicates that the preulcer area became ischemic relative to nearby unaffected tissue as the callus grew. Indeed, an increase in epidermal thickness (callus formation) may result in increased and irregular pressure on that part of the foot [38]. This may cause poor blood circulation and subsequent ulceration in the area [38]. In fact, our previous study [11] showed that a large increase or reduction in the local oxyhemoglobin concentration strongly correlates with risk of ulcer formation in that area. Note that the absolute values of deoxyhemoglobin concentration during these visits were 70, 54, 73, and 47 μM, respectively, and did not show a clear pattern as observed earlier [11].

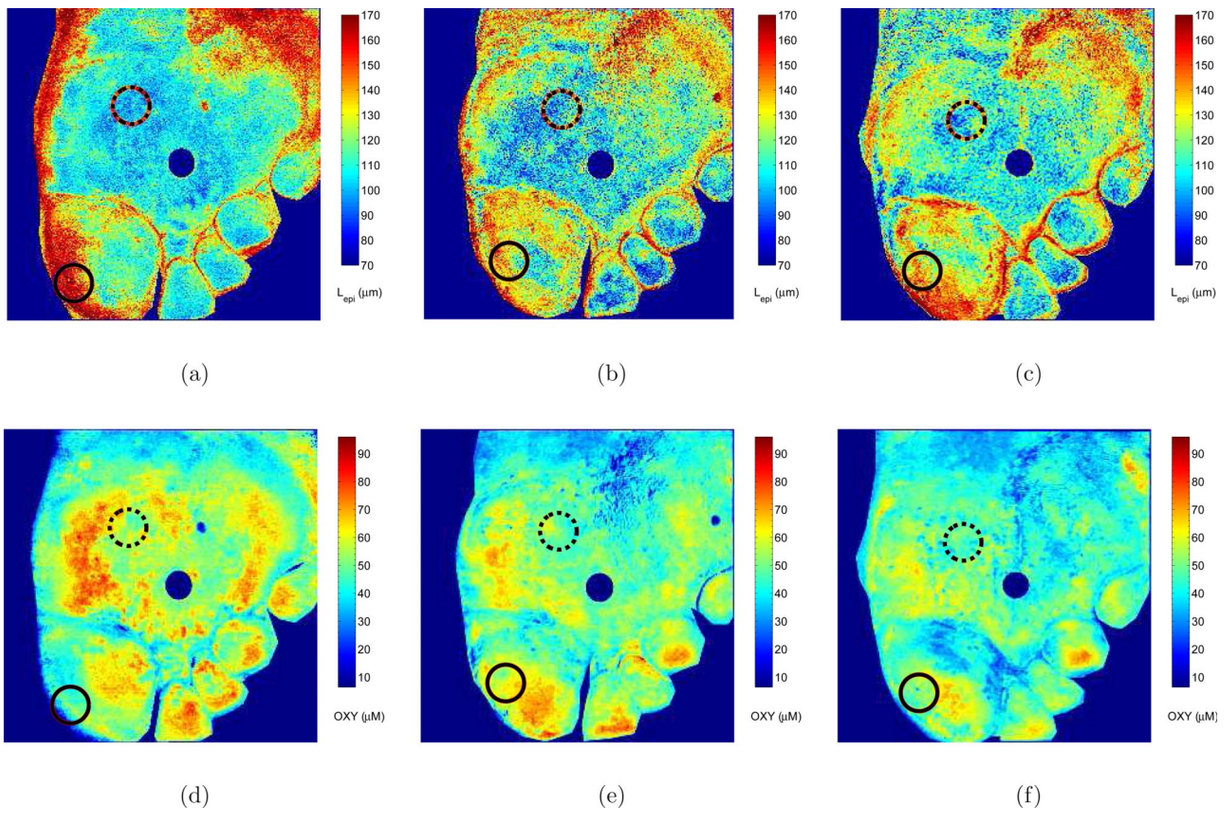

Figure 5 (online color at: www.biophotonics-journal.org) (**a**) to (**c**) Epidermal thickness and (**d**) to (**f**) oxyhemoglobin concentration maps during foot ulceration corresponding to images to maps shown in Figure 4. Solid line circle indicates the ulceration site. Dashed line circle indicates the control site.

Journal of
BIOPHOTONICS

Thus, the present analysis could enable one to gain insight into the mechanisms involved with ulcer formation. It suggests that as the callus grows, it causes pressure disturbances in the foot which affect the foot's circulatory function.

4.2 *Ulcer healing*

Figures 4 through 7 show results for the toes and plantar surface of the left foot of another diabetic patient collected over six visits during an eleven month period. Figure 4 shows the visible images and oxygen saturation maps of the patient's foot before the ulcer formed on the first digit. The oxygen saturation averaged over the entire foot decreases from 85% to 57% between visits 1 and 3 indicating poor circulation in the affected foot during the weeks leading up to ulceration. No significant differences were observed in oxygen saturation in the preulcer and control areas for the three visits. However, epidermal thickening (Figure 5) was observed on the first digit almost six months (Figure 5a) prior to visit 4 (Figure 6a) when the formed ulcer was clearly apparent on the visible images. In fact, the average epidermal thickness at the preulcer site was found to be 158, 132, and 138 μm during visits 1, 2, and 3 (Figures 5a through 5c), respectively. On the other hand, the average epidermal thickness in the control region (dashed circle) varied very little during the same visits and was 99, 102, and 103 μm, respectively. Simultaneously, oxyhemoglobin concentration was also elevated during the first three visits as evident in Figures 5d through 5f. However, elevation in oxyhemoglobin concentration occurred also on all the other toes and on the plantar surface and not only at the preulcer area. On the other hand, epidermal thickening and oxyhemoglobin concentration increased simultaneously on the first digit which subsequently ulcerated.

Moreover, Figures 6 and 7 show the visible images and maps of the patient's foot during healing. During visit 4 (Figure 6a), the open ulcer was approximately 2 cm in diameter and surrounded by a thick callus ring. The presence of callus was clearly apparent to the naked eye during visits 4 and 5 (Figures 6a and 6b). This was properly captured by our

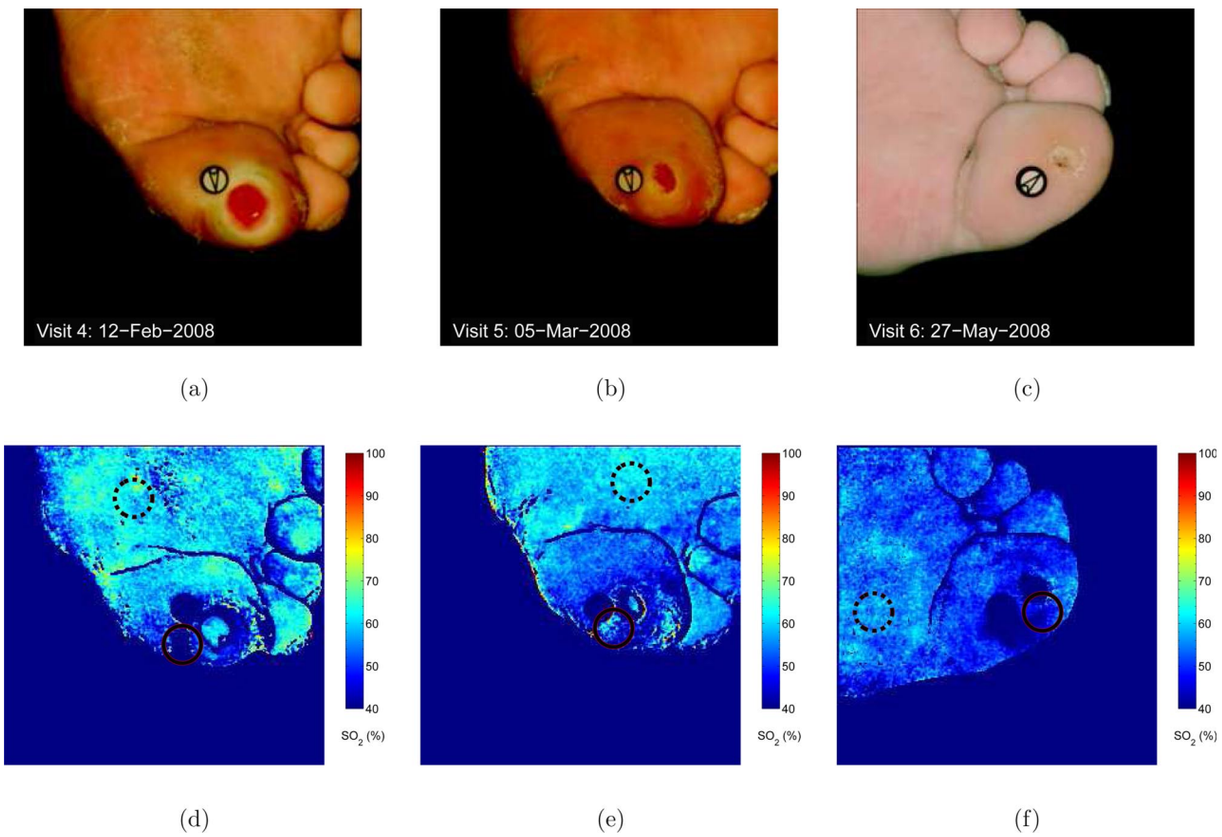

Figure 6 (online color at: www.biophotonics-journal.org) (**a**) to (**c**) Visible images and (**d**) to (**f**) oxygen saturation maps of the plantar surface of a diabetic subject during healing of the foot ulcer formed on the hallux of the left foot.

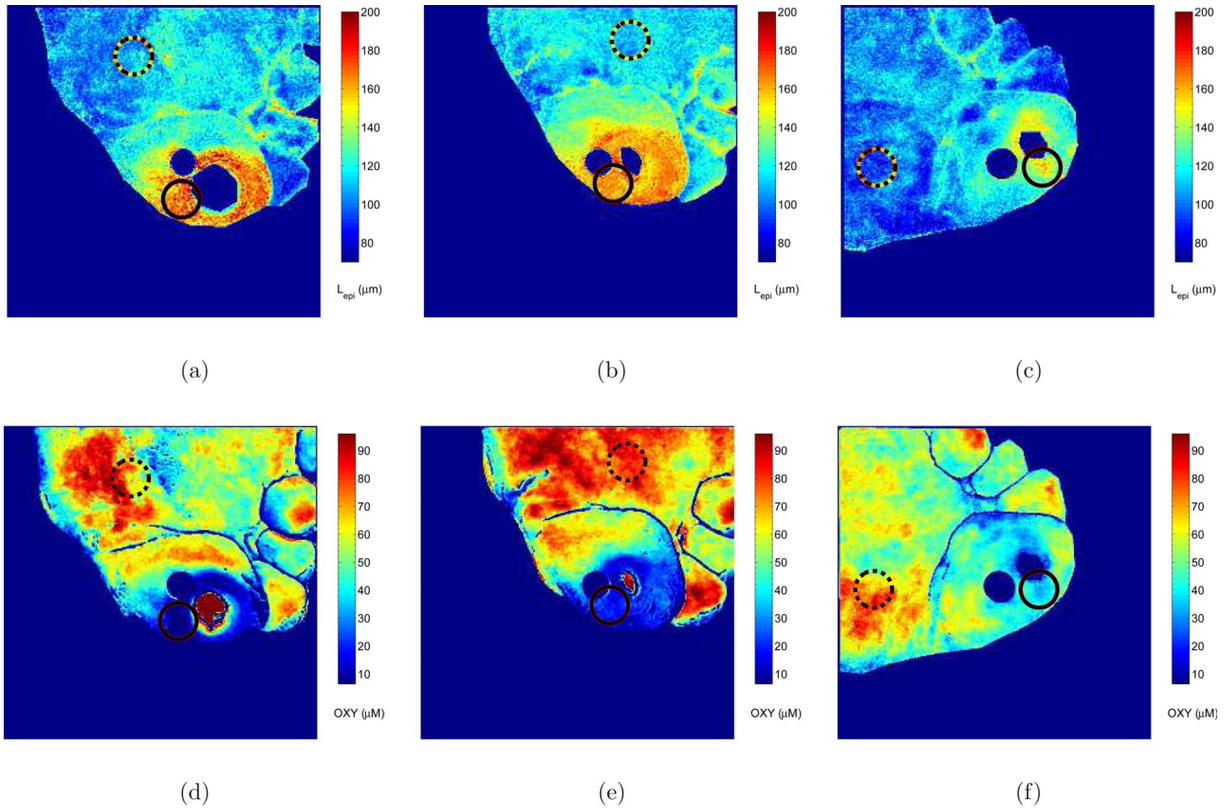

Figure 7 (online color at: www.biophotonics-journal.org) (**a**) to (**c**) Epidermal thickness and (**d**) to (**f**) oxyhemoglobin concentration maps during foot ulceration corresponding to images to maps shown in Figure 6. Solid line circle indicates the ulceration site. Dashed line circle indicates the control site.

algorithm as illustrated in Figure 7a and 7b. The average estimated epidermal thickness calculated in a 1 cm diameter circle positioned on the callus ring (solid line) was 167 and 163 μm during visits 4 and 5, respectively. Finally, Figure 7c establishes that, during the last visit, the region of epidermal thickening subsided around the ulcer as it healed and closed. In fact, the average epidermal thickness estimated in a 1 cm diameter circle centered on the callus decreased to 150 μm during the last visit. On the other hand, the epidermal thickness was 111, 108, and 92 μm at the control regions during visits 4, 5 and 6, respectively. These values were similar to those retrieved at the site before the ulcer formed. For reference, Figure 7d through 7f also show the oxyhemoglobin maps of the healing ulcer. Reduction in callus size and thickness between visits 4 and 6 evident from Figure 7a through 7c corresponds to improved circulation near the ulcer suggested by the increase in oxyhemoglobin concentration reported in Figure 7d through 7f.

Figure 8 summarizes the temporal progression of epidermal thickness in the preulcer and control

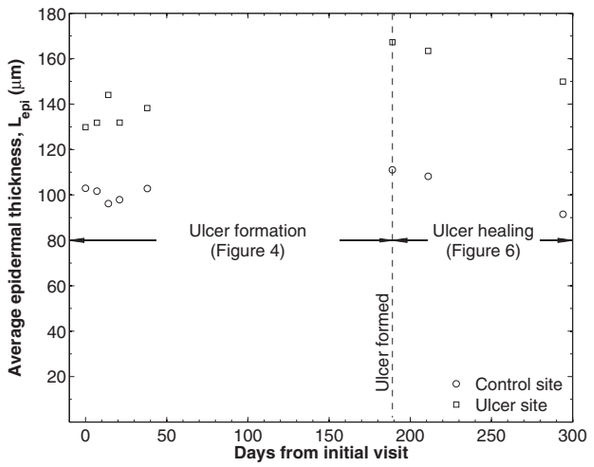

Figure 8 Average retrieved epidermal thickness as a function of days from the first visit on June 27, 2007 (visit 1) to May 27, 2008 (visit 6) calculated at the preulcer site (square) and at the control site (circle) for the foot shown in Figures 4 and 6.

Journal of
BIOPHOTONICS

areas, respectively, for all sets of hyperspectral images available for the second patient. Estimates of epidermal thickness gradually increased during ulcer formation and were 30 μm larger at the ulcer site than at a nearby control site. After the ulcer formed, the estimates of the epidermal thickness near the callus were consistently higher than in the same region prior to ulceration and decreased as the ulcer healed. During ulcer healing, both the ulcer and control sites show a decrease in epidermal thickness with time. Off-loading the affected foot is a typical treatment for diabetic foot ulceration. This may have resulted in epidermal thinning around the ulcer location, but also on the plantar surface of the foot where the control region was chosen.

4.3 Clinical implications

In a previous study, spatial variations in oxyhemoglobin and deoxyhemoglobin concentrations were used to detect tissue at risk of ulceration [11]. The average oxyhemoglobin and deoxyhemoglobin concentrations were found in a 1 cm diameter circular target region centered over a pixel and 8 adjacent regions. Then, the maximum difference between the averaged oxyhemoglobin concentrations calculated in the target regions with respect to the control regions was computed and denoted by MD(OXY). The MD(DEOXY) value was found in the same fashion. The MD(OXY) and MD(DEOXY) values were calculated for each pixel. Furthermore, it was found that if |MD(OXY)| and |MD(DEOXY)| simultaneously exceeded their respective threshold values, then the pixel could be classified as preulcerous with a high sensitivity and moderately high specificity. As depicted in Figures 2 through 7, ulcer formation is preceded by callus formation that results in a local increase in epidermal thickness. It is thus expected that values of MD(L_{epi}) calculated over preulcer regions would be larger on average than from surrounding unaffected regions.

In practice, the algorithm and methodology presented in this work can be applied directly to data gathered by a hyperspectral imager. To illustrate the clinical usefulness of detecting epidermal thickness on the feet of diabetic patients at risk of developing foot ulcer, the present technique should be applied to a larger population of patients, as performed in Ref. [11]. This task, however, falls outside the scope of the present study which focused on monitoring the evolution of foot ulcers from formation to healing for two specific patients.

5. Conclusion

Hyperspectral imaging of the feet of two diabetic patients was performed before, during, and after they developed foot ulcer. Previous studies of diabetic foot ulcer formation using hyperspectral imaging limited their analysis to circulatory changes such as difference in oxyhemoglobin and deoxyhemoglobin concentrations obtained from hyperspectral images collected immediately prior to foot ulcer formation or immediately following ulcer healing [10, 11, 20, 21]. The present study examined the temporal changes observed before the ulcer became apparent to the naked eye until it healed and closed. Epidermal thickening was observed in preulcerous areas which is consistent with callus formation in such regions. The callus was observed to recede as the ulcer healed. The corresponding increase in local epidermal thickness was associated with a decrease in oxyhemoglobin concentration. This study establishes the feasibility of using measurements of epidermal thickness to enhance other imaging modalities, in particular hyperspectral tissue oximetry [11], for early prediction of diabetic foot ulcer formation.

Acknowledgements This research was funded in part through a grant from the National Institute of Diabetes and Digestive and Kidney Diseases (R42-DK069871).

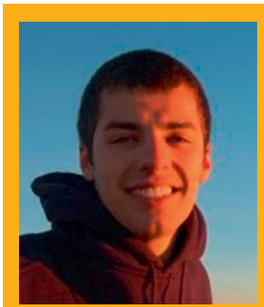

Dmitry Yudovsky received his B.S. in Mechanical Engineering at the University of California, San Diego in 2006. He pursued his graduate studies at the University of California, Los Angeles where he received a M.S. and a Ph.D. in 2008 and 2010, respectively. He is currently a Postdoctoral Research at the Beckman Laser Institute at the University of California, Irvine. His research interests include biomedical imaging, optical tissue modeling and non-invasive tissue health-monitoring.

Aksone Nouvong graduated from the University of California, Santa Barbara with a BA in Biology. She received the degree of Doctor of Podiatric Medicine from the California College of Podiatric Medicine, San Francisco, CA. She completed her residency training at the DVA Greater Los Angeles and Olive View – UCLA Medical Center. Dr. Nouvong is an Assistant Clinical Professor in the Department of General Surgery the David Geffen School of Medicine at UCLA and serves as the Assistant Dean of Clinical Affairs at Western University of Health Sciences, College of Podiatric Medicine.

Kevin Schomacker received his B.S. in Chemistry from Worcester State College in 1981 and his Ph.D. in Chemical Physics from Northeastern University in 1987. In 1988, he joined Wellman Laboratories of Photomedicine at Massachusetts General Hospital where he advanced to an Associate Physicist in Dermatology with a joint appointment as Assistant Professor in Dermatology at the Harvard Medical School. In 2001, he joined MediSpectra Inc. as their Director of Research and in 2005 he moved to HyperMed Inc. as their Vice President of Research and Clinical Development. Since 2009, he serves as the Director of New Applications for Candela Corporation.

Laurent Pilon received his B.S. and M.S. in Applied Physics in 1997 from the Grenoble Institute of Technology, France and a Ph.D. in Mechanical Engineering from Purdue University in 2002. He then joined the Henry Samueli School of Engineering at UCLA where he is now Associate Professor with affiliations in the Mechanical and Aerospace Engineering Department and in the Biomedical Engineering Interdepartmental Program. He has authored more than 60 archival journal publications on biophotonics, radiation transfer, applied optics, and thermal sciences.

References

[1] S. Wild, G. Roglic, A. Green, R. Sicree, and H. King, Diabetes Care **27**, 1047–1053 (2004).
[2] J. E. Shaw, R. A. Sicree, and P. Z. Zimmet, Diabetes Res. and Clin. Pract. **87**, 4–14 (2010).
[3] G. E. Reiber, Diabet. Med. **13**, 6–11 (1996).
[4] A. J. M. Boulton, D. G. Armstrong, S. F. Albert, R. G. Frykberg, R. Hellman, M. S. Kirkman, L. A. Lavery, J. W. LeMaster, J. L. Mills Sr., J. W. Lemaster, M. J. Mueller, P. Sheehan, and D. K. Wukich, Diabetes Care **31**, 1679–1685 (2008).
[5] C. Harrington, M. J. Zagari, J. Corea, and J. Klitenic, Diabetes Care **23**, 1333–1338 (2000).
[6] S. D. Ramsey, K. Newton, D. Blough, D. K. McCulloch, N. Sandhu, G. E. Reiber, and E. H. Wagner, Diabetes Care **22**, 382–387 (1999).
[7] R. E. Pecoraro, G. E. Reiber, and E. M. Burgess, Diabetes Care **13**, 513–521 (1990).
[8] R. G. Frykberg, T. Zgonis, D. G. Armstrong, V. R. Driver, J. M. Giurini, S. R. Kravitz, A. S. Landsman, L. A. Lavery, J. C. Moore, J. M. Schuberth et al., J. Foot Ankle Surg. **45**, 1–66 (2006).
[9] R. L. Greenman, S. Panasyuk, X. Wang, T. E. Lyons, T. Dinh, L. Longoria, J. M. Giurini, J. Freeman, L. Khaodhiar, and A. Veves, Lancet **366**, 1711–1717 (2005).
[10] A. Nouvong, B. Hoogwerf, E. Mohler, B. Davis, A. Tajaddini, and E. Medenilla, Diabetes Care **32**, 2056–2061 (2009).
[11] D. Yudovsky, A. Nouvong, K. Schomacker, and L. Pilon, J. Biomed. Opt. 2010 (accepted).
[12] A. J. M. Boulton, Medicine **34**, 87–90 (2006).
[13] A. P. Brooks, Diabet. Med. **3**, 116–118 (1986).
[14] H. M. Rathur and A. J. M. Boulton, Clin. Dermatol. **25**, 109–120 (2007).
[15] L. Belbridge, G. Ctercteko, C. Fowler, T. S. Reeve, and L. P. Le Quesne, Br. J. Surg. **72**, 1–6 (1985).
[16] P. J. Palumb and L. J. Melton, Chapter 17. Peripheral vascular disease and diabetes, in M. I. Harris and R. F. Hamman (eds.), Diabetes in America, 401–408. (U. S. Government Printing Office, Washington, DC, 2nd edition, 1995) NIH publication 851468.
[17] J. C. Finlay and T. H. Foster, Med. Phys. **31**, 1949–1959 (2004).
[18] K. J. Zuzak, M. D. Schaeberle, E. N. Lewis, and I. W. Levin, Anal. Chem. **74**, 2021–2028 (2002).
[19] P. J. Dwyer and C. A. DiMarzio, Proc. SPIE 3752, 72–82 (1999).
[20] L. Khaodhiar, T. Dinh, K. T. Schomacker, S. V. Panasyuk, J. E. Freeman, R. Lew, T. Vo, A. A. Panasyuk, C. Lima, J. M. Giurini, T. E. Lyons, and A. Veves, Diabetes Care **30**, 903–910 (2007).
[21] R. Gillies, J. E. Freeman, L. C. Cancio, D. Brand, M. Hopmeier, and J. R. Mansfield, Diabetes Technol. Ther. **5**, 847–855 (2003).
[22] D. Yudovsky and L. Pilon, Appl. Opt. **48**, 6670–6683 (2009).
[23] D. Yudovsky and L. Pilon, Appl. Opt. **49**, 1707–1719 (2010).

[24] D. Yudovsky and L. Pilon, J. Biophotonics **3**, 1–10 (2010).
[25] Y. Lee and K. Hwang, Surg. Radiol. Anat. **24**, 183–189 (2002).
[26] J. Sandby-Moller, T. Poulsen, and H. C. Wulf, Acta Dermato-Venereol. **83**, 410–413 (2003).
[27] T. Gambichler, R. Matip, G. Moussa, P. Altmeyer, and K. Hoffmann, J. Dermatol. Sci. **44**, 145–152 (2006).
[28] P. P. Guastalla, V. I. Guerci, A. Fabretto, F. Faletra, D. L. Grasso, E. Zocconi, D. Stefanidou, P. D'Adamo, L. Ronfani, M. Montico et al., Radiology **251**, 280 (2009).
[29] D. J. Faber and T. G. van Leeuwen, Opt. Lett. **34**, 1435–1437 (2009).
[30] D. J. Faber, E. G. Mik, M. C. G. Aalders, and T. G. van Leeuwen, Opt. Lett. **30**, 1015–1017 (2005).
[31] M. F. Modest, Radiative Heat Transfer (Academic Press, San Diego, CA, 2003).
[32] L. B. Wolff, J. Opt. Soc. Am. **11**, 2956–2968 (1994).
[33] M. Singh, Med. Biol. Engin. Comput. **19**, 175–178 (1981).
[34] J. D. Hardy, H. T. Hammel, and D. Murgatroyd, J. Appl. Physiol. **9**, 257–264 (1956).
[35] D. W. Marquardt, J. Soc. Indust. Appl. Math. **11**, 431–441 (1963).
[36] A. R. Young, Phys. Med. Biol., **42**, 789–802 (1997).
[37] M. C. Branchet, S. Boisnic, C. Frances, and A. M. Robert, Gerontology **36**, 28–35 (1990).
[38] J. A. Birke, A. Novick, E. S. Hawkins, and C. Patout Jr., J. Prosthet. Orthot. **4**, 13–22 (1991).

